

MIT Open Access Articles

Roles of H3K27me2 and H3K27me3 Examined during Fate Specification of Embryonic Stem Cells

The MIT Faculty has made this article openly available. **Please share** how this access benefits you. Your story matters.

Citation: Juan, Aster H. et al. "Roles of H3K27me2 and H3K27me3 Examined during Fate Specification of Embryonic Stem Cells." Cell Reports 17.5 (2016): 1369–1382. © 2017 Elsevier

As Published: <http://dx.doi.org/10.1016/j.celrep.2016.09.087>

Publisher: Elsevier

Persistent URL: <http://hdl.handle.net/1721.1/107488>

Version: Final published version: final published article, as it appeared in a journal, conference proceedings, or other formally published context

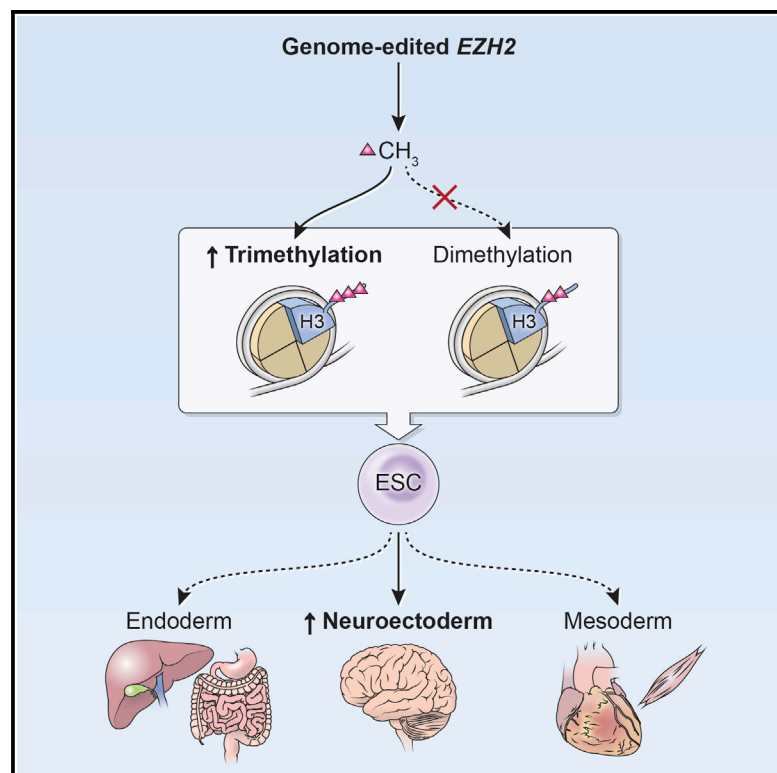
Terms of use: Creative Commons Attribution-NonCommercial-NoDerivs License



Cell Reports

Roles of H3K27me2 and H3K27me3 Examined during Fate Specification of Embryonic Stem Cells

Graphical Abstract



Authors

Aster H. Juan, Stan Wang, Kyung Dae Ko, ..., Rafael Casellas, Jizhong Zou, Vittorio Sartorelli

Correspondence

juana2@mail.nih.gov (A.H.J.), sartorev@mail.nih.gov (V.S.)

In Brief

Juan et al. use genome editing to subtly modify H3K27 methylation states (H3K27me2/H3K27me3) and report that such perturbation influences the ability of ESCs to differentiate into preferential cell lineages and acquire a “ground state.”

Highlights

- H3K27me2/H3K27me3 are redistributed during ESC differentiation
- H3K27 methylation recapitulates changes during differentiation in Ezh2-edited ESCs
- In pluripotent culture conditions, Ezh2-edited ESCs activate the neurogenic program
- Ezh2-edited ESCs are refractory to a 2i-medium-induced “ground state”

Accession Numbers

GSE85717



Juan et al., 2016, Cell Reports 17, 1369–1382
October 25, 2016
<http://dx.doi.org/10.1016/j.celrep.2016.09.087>

CellPress

Roles of H3K27me2 and H3K27me3 Examined during Fate Specification of Embryonic Stem Cells

Aster H. Juan,^{1,10,*} Stan Wang,^{1,2,3,10,11} Kyung Dae Ko,¹ Hossein Zare,¹ Pei-Fang Tsai,¹ Xuesong Feng,¹ Karinna O. Vivanco,^{1,4} Anthony M. Ascoli,¹ Gustavo Gutierrez-Cruz,¹ Jordan Krebs,⁵ Simone Sidoli,⁶ Adam L. Knight,⁷ Roger A. Pedersen,^{3,8} Benjamin A. Garcia,⁶ Rafael Casellas,⁵ Jizhong Zou,⁹ and Vittorio Sartorelli^{1,12,*}

¹Laboratory of Muscle Stem Cells and Gene Regulation, National Institute of Arthritis, Musculoskeletal and Skin Diseases (NIAMS), National Institutes of Health, Bethesda, MD 20892, USA

²Wellcome Trust/Cancer Research UK Gurdon Institute, Tennis Court Road, Cambridge CB2 1QN, UK

³Department of Surgery, University of Cambridge, Cambridge CB2 0QQ, UK

⁴Department of Biological Engineering, Massachusetts Institute of Technology, 77 Massachusetts Avenue, Cambridge, MA 02139, USA

⁵Genomics and Immunity, NIAMS, National Institutes of Health, Bethesda, MD 20892, USA

⁶Epigenetics Program, Department of Biochemistry and Biophysics, Perlman School of Medicine, University of Pennsylvania, Philadelphia 19104 PA, USA

⁷Synaptic Function Section, The Porter Neuroscience Research Center, National Institute of Neurological Disorders and Stroke, National Institutes of Health, Bethesda, MD 20892, USA

⁸The Anne McLaren Laboratory for Regenerative Medicine, University of Cambridge, Downing Street, Cambridge, CB2 3EH, UK

⁹iPSC Core Facility, Center for Molecular Medicine, National Heart, Lung and Blood Institute, National Institutes of Health, Bethesda, MD 20892, USA

¹⁰Co-first author

¹¹Present address: Columbia University College of Physicians and Surgeons, 630 West 168th Street, New York, NY 10032, USA

¹²Lead Contact

*Correspondence: juana2@mail.nih.gov (A.H.J.), sartorev@mail.nih.gov (V.S.)

<http://dx.doi.org/10.1016/j.celrep.2016.09.087>

SUMMARY

The polycomb repressive complex 2 (PRC2) methylates lysine 27 of histone H3 (H3K27) through its catalytic subunit Ezh2. PRC2-mediated di- and trimethylation (H3K27me2/H3K27me3) have been interchangeably associated with gene repression. However, it remains unclear whether these two degrees of H3K27 methylation have different functions. In this study, we have generated isogenic mouse embryonic stem cells (ESCs) with a modified H3K27me2/H3K27me3 ratio. Our findings document dynamic developmental control in the genomic distribution of H3K27me2 and H3K27me3 at regulatory regions in ESCs. They also reveal that modifying the ratio of H3K27me2 and H3K27me3 is sufficient for the acquisition and repression of defined cell lineage transcriptional programs and phenotypes and influences induction of the ESC ground state.

INTRODUCTION

Polycomb repressive complex 2 (PRC2) is essential for H3K27 methylation (Margueron and Reinberg, 2011) and exerts important functions in ESCs and induced pluripotent stem cells (iPSCs; Boyer et al., 2006; Chamberlain et al., 2008; Lee et al., 2006; Leeb et al., 2010; Montgomery et al., 2005; Pasini et al., 2007; Shen et al., 2008; Onder et al., 2012; Riising et al., 2014).

Their genome-wide distribution and distinct enrichment suggest different functions for the individual H3K27 methylation states (Cui et al., 2009; Steiner et al., 2011; Azuara et al., 2006; Bernstein et al., 2006; Boyer et al., 2006; Lee et al., 2006; Shen et al., 2009). While H3K27me3 and H3K27me1 have been associated with gene repression and activation, respectively (Margueron and Reinberg, 2011; Cui et al., 2009; Ferrari et al., 2014), the role of H3K27me2 has remained less explored. Recent studies conducted in temperature-sensitive mutant *E(z)⁶¹* *Drosophila* EZ2-2 cells (Lee et al., 2015) and in PRC2 (*Eed^{-/-}*) knockout ESCs attribute a role to H3K27me2 in preventing inappropriate enhancer activation (Ferrari et al., 2014). The proposed function of H3K27me2 in restricting random and unscheduled transcription throughout the genome predicts its developmentally regulated distribution at distinct regulatory regions. However, the temporal dynamics of H3K27me2 in ESCs are unclear. Thus, the question of whether maintenance of an appropriate balance between H3K27me2 and H3K27me3 is relevant for the regulation of gene expression and acquisition of distinct cell fates remains unanswered. Perturbation of the H3K27me2/H3K27me3 ratio, without altering PRC2 stoichiometry, may directly address the function of these two degrees of H3K27 methylation. Mutation of the PRC2 subunit Ezh2 tyrosine 641 to phenylalanine (Ezh2Y641F), occurring in B cell lymphomas and melanomas (Yap et al., 2011; McCabe et al., 2012; Barsotti et al., 2015; Souroullas et al., 2016), results in markedly improved H3K27 trimethylase activity, possibly via a Phe/Tyr switch mechanism (Collins et al., 2005).

Here, we exploit these biochemical properties and introduce the Y641F mutation in one of the two *Ezh2* alleles of ESCs via

transcription activator-like effector nuclease (TALEN)-mediated genome editing. We document specific and dynamic genome-wide distribution of H3K27me2 and H3K27me3 in undifferentiated and differentiating ESCs and find that modification of the H3K27me2/H3K27me3 ratio results in the acquisition and repression of defined cell lineages, as well as influencing the induction of the ESC ground state.

RESULTS

Distinct H3K27 Methylation States Are Enriched at Functionally Defined Genomic Regulatory Regions of Different Classes of Genes in ESCs

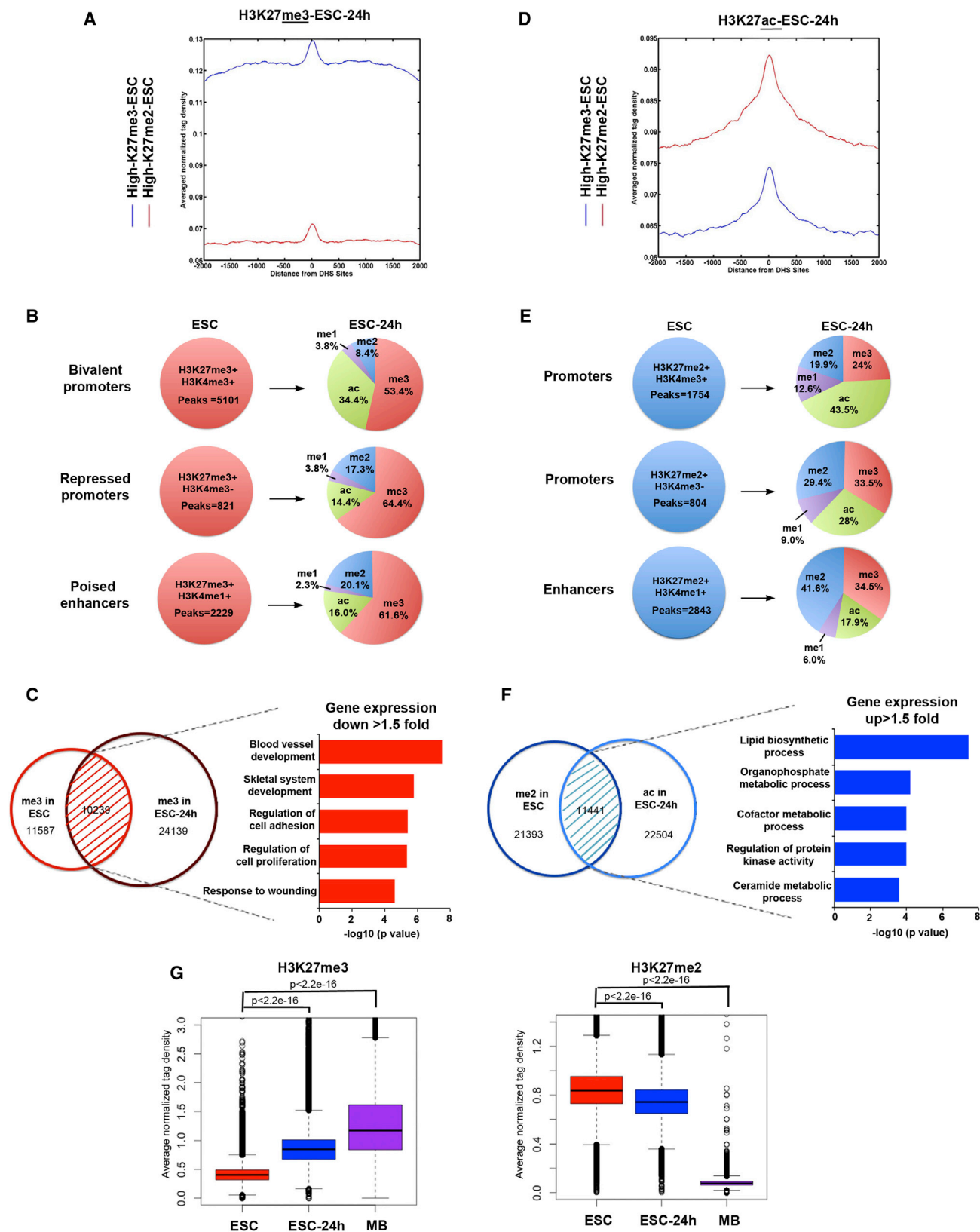
We surveyed the genome-wide distribution of the three H3K27 methylation states (H3K27me1, H3K27me2, and H3K27me3) in mouse ESCs by chromatin immunoprecipitation followed by sequencing (ChIP-seq). Antibody specificities were documented by dot blot and immunoprecipitation-immunoblot assays with a battery of antibodies recognizing different degrees of H3K27 methylation (Figure S1A). The number of replicates, computed peaks for the histone marks, and RNA sequencing (RNA-seq) reads are reported in Figure S1B. Analysis of the ChIP-seq datasets revealed that ~27% of H3K27me3, ~8% of H3K27me2, and 20% of H3K27me1 peaks were enriched at promoter regions, respectively (Figure S2A). H3K27me1 was enriched at transcription start sites (TSSs) and in gene bodies (Figure S2B). Different percentages of H3K27 methylation were also observed at intragenic regions: ~64% of H3K27me1, 44% of H3K27me2, and 30% of H3K27me3 signals (Figure S2A). Similar percentages of H3K27me3 and H3K27me2 (~42% and ~47%, respectively) were found at intergenic regions, whereas this genomic compartment hosted only ~15% of H3K27me1 peaks (Figure S2A). To gain initial insight into the regulatory regions occupied by H3K27me2 and H3K27me3, we positioned their respective averaged normalized tag densities at TSSs or genomic regions characterized by the presence of DNase-I-hypersensitive sites (DHSs) derived from a collection of publicly available DHS datasets in ESCs, different somatic cells, and tissues (see [Experimental Procedures](#)). TSSs were excluded from the considered DHSs, which therefore are likely to encompass prospective active regulatory regions. The H3K27me3 signal was mainly enriched at regions immediately surrounding the TSS (± 1 kb) (Figure S2C, blue trace), whereas H3K27me2 preferentially accumulated at prospective DHS regions (Figure S2D, red trace). To further define the genomic location of H3K27 methylation, we intersected H3K27me1, H3K27me2, or H3K27me3 peaks with either H3K4me3 at TSSs (H3K4me3⁺/TSSs) or H3K4me1, a histone mark preferentially enriched at distant regulatory regions (Heintzman et al., 2007). The bulk of H3K27me3⁺/TSSs (~88%) were H3K4me3⁺, whereas comparably fewer H3K27me2⁺/TSSs (~55%) were co-occupied by H3K4me3. More than 90% of the H3K27me1 signal occurred at H3K4me3⁺/TSSs (Figure S2E). At H3K4me1⁺ regions, the percentages of H3K27me3⁺ regions and H3K27me2⁺ regions were similar (~44% and 48%, respectively), whereas H3K27me1 was less represented (~27%) (Figure S2F). To evaluate whether the catalytic PRC2 subunit Ezh2 was differentially enriched at H3K27me3 and H3K27me2 regions, we conducted Ezh2 ChIP-

seq experiments. Scatterplot analysis revealed a positive correlation for H3K27me3 and negative correlation for H3K27me2 with Ezh2 binding (Figure S3A). Both H3K27me3 and H3K27me2 regions were equally enriched for guanines and cytosines and displayed enrichment for a similar set of DNA-binding motifs (Figures S3B and S3C).

Next, we investigated the transcriptional state of H3K27me3⁺, H3K27me2⁺, and H3K27me1⁺ genes. The majority of H3K27me3⁺ genes were repressed or expressed at low levels (reads per kilobase of transcription per million [RPKM] < 1) (53%), and the remaining 47% were expressed at higher levels (RPKM > 1). H3K27me3⁺ genes with higher expression (RPKM > 1) were enriched for early developmental processes, whereas lowly expressed genes (RPKM < 1) encompassed those involved in cell-cell signaling, neuron differentiation, and cell fate commitment (Figure S2G; Tables S1 and S2). H3K27me2⁺ genes were mainly expressed at higher levels (~64%, RPKM > 1) and corresponded to metabolic processes (Figure S2H; Tables S1 and S2). Lowly expressed (RPKM < 1) H3K27me2⁺ genes identified terms related to immune responses (Figure S2H; Tables S1 and S2). More than 90% of the H3K27me1⁺ genes were highly expressed and corresponded to those involved in non-coding RNA metabolic processes (rRNA and tRNA), cellular responses to stress, and cell-cycle control (Figure S2I). Overall, these data indicate that in ESCs, H3K27me3, H3K27me2, and H3K27me1 are distributed at distinct genomic regions and are associated with genes related to discrete biological processes in different transcriptional states.

Developmental Dynamics of H3K27 Methylation States in ESCs

To assess the developmental dynamics of H3K27 post-translational modifications (PTMs), we conducted ChIP-seq for H3K27me3, H3K27me2, H3K27me1, and H3K27 acetylation (ac) in ESCs cultured in conditions either maintaining pluripotency (high serum, on feeders, with leukemia inhibitory factor [LIF]) or inducing differentiation (cultured for 24 hr at low density, without serum and without LIF). Regions with the highest H3K27me3 enrichment (top quartile) in pluripotent ESCs preferentially retained this histone modification in differentiating ESCs, whereas H3K27me2⁺ regions were less likely to acquire H3K27me3 (Figure 1A). H3K27me3 was intersected with H3K4me3⁺/TSSs and H3K4me1⁺ maps. Approximately 53% of bivalent genes (H3K27me3⁺/H3K4me3⁺) retained H3K27me3⁺ upon differentiation (Figure 1B, top). The percentage of H3K27me3⁺ retention in differentiating ESCs was higher at repressed regions (64% at H3K27me3⁺/H3K4me3⁻ regions; Figure 1B, middle) and poised enhancers (61% at H3K27me3⁺/H3K4me1⁺ regions; Figure 1B, bottom). In differentiating ESCs, H3K27me3 was retained at genomic regions associated (± 20 kb from TSSs) with repressed genes related to developmental processes (Figure 1C; Table S3). In contrast to H3K27me3 (Figure 1D, blue trace), regions with the highest H3K27me2 enrichment in pluripotent ESCs were more prone to acquire H3K27ac during differentiation (Figure 1D, red trace). H3K27me2 displayed more dynamic behavior than H3K27me3, with ~43% of H3K27me2⁺/H3K4me3⁺/TSSs and ~28% H3K27me2⁺/H3K4me3⁻ regions becoming H3K27ac (Figure 1E,



(legend on next page)

top and middle, respectively). Intriguingly, a similar percentage of poised enhancers (~16%; [Figure 1B](#) bottom) and H3K27me2⁺/H3K4me1⁺ regions (~18%; [Figure 1E](#), bottom) transitioned to H3K27ac in differentiating ESCs. Thus, while occurring at enhancers ([Ferrari et al., 2014](#)), an H3K27me2-to-H3K27ac switch was more prevalent at promoters. Regulatory regions undergoing this switch were located in the vicinity (± 20 kb from TSSs) of upregulated genes related to metabolic processes ([Figure 1F](#); [Table S3](#)). Compared to pluripotent ESCs, the average normalized tag density of intergenic H3K27me3 peaks was increased in both ESC differentiated for 24 hr (ESC-24h) and more differentiated somatic cells (skeletal myoblast [MB]) ([Figure 1G](#), left). Conversely, the intergenic H3K27me2 signal was decreased in ESC-24h and, more profoundly, in skeletal myoblasts ([Figure 1G](#), right). Almost half (~48%) of H3K27me1⁺/H3K4me3⁺/TSS regions acquired H3K27ac in differentiating ESCs ([Figure S3D](#), top) whereas similar H3K27ac percentages were observed for H3K27me1⁺/H3K4me3⁻ and H3K27me1⁺/H3K4me1⁺ regions, respectively ([Figure S3D](#), middle and bottom). Average normalized H3K27me1 tag density was comparable in pluripotent and differentiating ESCs ([Figure S3E](#)). Collectively, these data indicate that during ESC differentiation, H3K27me3, H3K27me2, and H3K27me1 are dynamically redistributed at regulatory regions of distinct classes of genes.

TALEN-Mediated Genome Editing of *Ezh2* Modifies H3K27me2 and H3K27me3 in ESCs

To perturb H3K27 methylation, we generated isogenic ESCs via TALEN-mediated genome editing ([Bogdanove and Voytas, 2011](#)) of the *Ezh2* coding region, causing the replacement of Tyr641 with phenylalanine (Y641F) ([Figure 2A](#)). This mutation, detected in a subset of B cell lymphomas and melanomas, results in the formation of Ezh2Y641F-containing PRC2 complexes with increased enzymatic activity on H3K27me2 substrates, thereby shifting the steady state of H3K27 to favor in vivo trimethylation ([Yap et al., 2011](#); [McCabe et al., 2012](#); [Barsotti et al., 2015](#); [Souroullas et al., 2016](#)). Maintenance of one *Ezh2* wild-type allele ensures generation of H3K27 mono- and dimethylated substrates upon which Ezh2Y641F can act ([Yap et al., 2011](#)). To confirm that Ezh2 genome editing in ESCs would recapitulate H3K27 methylation modifications observed in neoplastic cells, we performed immunoblot analysis of cytoplasmic, along with nuclear-

soluble and insoluble (chromatin), fractions and found decreased H3K27me2 and increased H3K27me3 histones in Y641F compared to wild-type (WT) ESCs in the chromatin nuclear-insoluble fraction (NI) ([Figure 2B](#)). These findings were substantiated by quantitative liquid chromatography-tandem mass spectrometry (LC-MS/MS) analysis documenting diminished H3K27me2 in Y641F ESCs ([Figure S4A](#)). Increased H3K27me3 in Y641F ESCs occurred at the histone variant H3.3 ([Figure S4A](#)), which is required for proper establishment of H3K27me3 at the promoters of developmentally regulated genes of ESCs ([Banaszynski et al., 2013](#)). H3K27me1 was not significantly affected by Y641F ([Figures S4A and S4C](#)). The levels of the PRC2 subunits Ezh2, Suz12, and Eed were comparable in WT and Y641F ESCs ([Figures 2B and 2C](#)). Similar biochemical features were observed in two independently isolated Y641F ESC clones ([Figure S4B](#)). To study their genomic distribution, we performed H3K27me2 and H3K27me3 ChIP-seq in WT and Y641F ESCs. Since H3K27me1 was not modified in Y641F ESCs, we did not further pursue this methylation state. Averaged tag density of H3K27me3 was increased in Y641F ESCs at a genomic interval encompassing an area ± 5 kb surrounding the TSS ([Figure 2D](#)), whereas within the same genomic intervals, H3K27me2 was decreased ([Figure 2E](#)). A similar analysis performed by centering H3K27 methylation peaks at prospective DHS regions confirmed increased H3K27me3 and decreased H3K27me2 in Y641F ESCs ([Figures 2F and 2G](#)).

H3K27me2 and H3K27me3 States of *Ezh2*-Edited ESCs Resemble Those of Differentiated ESCs

We next sought to compare the genomic distribution of H3K27me2 and H3K27me3 in pluripotent and differentiating ESC-24h, embryoid bodies (EBs), and Y641F ESCs. For this, WT and Y641F ESCs were cultured in conditions favoring maintenance of pluripotency. Alternatively, serum and LIF were withdrawn for 24 hr from ESCs (ESC-24h), and EBs (day 8) were derived from WT ESCs.

Principal-component analysis (PCA) was employed to measure and visualize differences in H3K27me2 and H3K27me3 maps between different ESC states in distinct genomic windows (PCA1, PCA2, and PCA3). This analysis permitted an effective segregation of the different ESC states, as depicted by 3D projections ([Figures 3A and 3C](#)). H3K27me2 PCA maps revealed that Y641F ESCs cultured in pluripotent conditions clustered closer to ESC-24h than to pluripotent ESCs ([Figure 3A](#)).

Figure 1. Dynamic Distribution of H3K27 Methylation States during ESC Differentiation

- (A) Average normalized tag density profiles depicting H3K27me3 enrichment in ESC-24h for prospective DHS regions within the top quartile of either H3K27me3⁺ (blue trace) or H3K27me2⁺ (red trace) in pluripotent ESCs.
- (B) Transition of H3K27me3 across bivalent versus repressed promoters and poised enhancers in ESC to different H3K27 states during early ESC differentiation (ESC-24h).
- (C) GO-biological processes associated with genes within ± 20 kb of H3K27me3⁺ regions in ESCs that maintain their H3K27me3 status in ESC-24h (shadowed area). Expression cutoff ≥ 1.5 -fold.
- (D) Average normalized tag density profiles depicting H3K27 acetylation enrichment in ESC-24h for prospective DHS regions within the top quartile of either H3K27me3⁺ (blue trace) or H3K27me2⁺ (red trace) in pluripotent ESCs.
- (E) Transition of H3K27me2 across H3K4me3^{+/−} promoters and H3K4me1⁺ enhancers in ESCs to different H3K27 states during early ESC differentiation (ESC-24h).
- (F) GO-biological processes associated with genes within ± 20 kb of H3K27me2⁺ regions in ESCs that acquire H3K27ac in ESC-24h (shadowed area). Expression cutoff ≥ 1.5 -fold.
- (G) Boxplot of H3K27me3 (left) and H3K27me2 (right) peak intensities for ± 5 -kb intergenic genomic regions surrounding the summit of each peak at two different ESC developmental stages and in skeletal myoblasts (MBs). p values were determined by Student's t test.

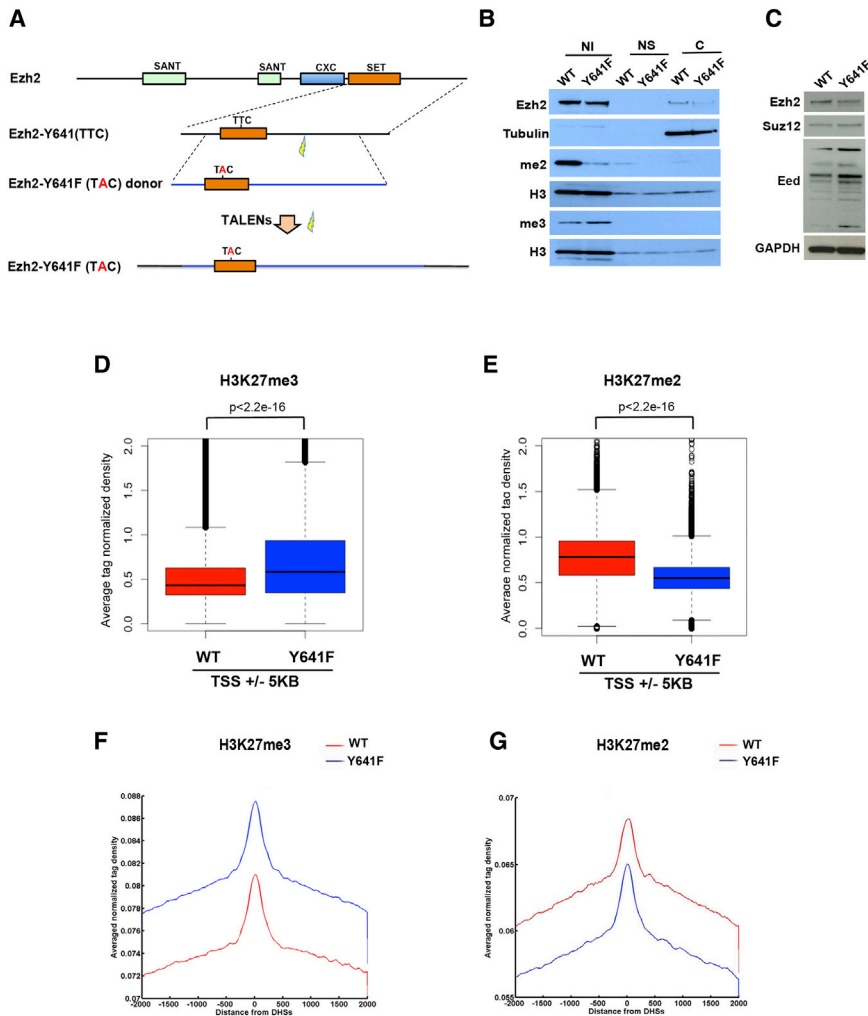


Figure 2. TALEN-Mediated Genome Editing of *Ezh2* Modifies H3K27me2 and H3K27me3 in ESCs

(A) Illustration of TALEN-mediated genome editing creating the *Ezh2*Y641F allele in ESCs. (B) Western blot for *Ezh2*, tubulin, H3K27me2 (me2), H3K27me3 (me3), and total histone H3 in WT or Y641F ESC chromatin fractions. NI, nuclear-insoluble fraction; NS, nuclear-soluble fraction; C, cytoplasmic fraction. (C) Western blot for PRC2 components *Ezh2*, *Suz12*, and *Eed* in WT or Y641F ESC whole-cell lysates. (D and E) Boxplots of H3K27me3 (D) and H3K27me2 (E) peak intensities for genomic regions surrounding (± 5 kb) TSSs in WT and Y641F ESCs. *p* values were determined by Student's *t* test. (F and G) Averaged normalized tag density profiles of H3K27me3 (F) or H3K27me2 (G) for genomic regions surrounding (± 2 kb) prospective DHS regions.

to WT ESCs, the H3K27me3 signal in both ESC-24h and Y641F ESCs spreads laterally from the TSS and invades intergenic regions (Figures 3E–3G). In agreement with the H3K27me3 PCA results (Figure 3A), genomic H3K27me3 distribution in ESC-24h was more similar to that of Y641F ESCs than WT ESCs, with reduced representation at promoters and increased occupancy of intergenic regions (Figures 3F and 3G). Altogether, these findings reveal that H3K27me2 and H3K27me3 maps of Y641F ESCs resemble those of ESCs undergoing differentiation. This observation

is in line with previous reports documenting that pluripotent ESCs have lower H3K27me3 levels compared to more differentiated cells (Hawkins et al., 2010; Pauler et al., 2009; Zhu et al., 2013). Approximately half (50%) of the genes with reduced H3K27me2 in Y641F ESCs corresponded to those acquiring H3K27 acetylation (Figure 3B). When correlated with gene expression, Gene Ontology (GO) analysis of upregulated genes returned terms related to metabolic processes (Figure 3B; Table S4), similar to those identified in ESC-24h (Figure 1F; Table S3). H3K27me3 PCA maps indicated that Y641F ESCs clustered closer to EB8 and ESC-24h than to pluripotent ESCs (Figure 3C). H3K27me3 PCA maps of all ESC states and EBs were markedly segregated from those of somatic cells and tissue types (Figure 3C). The majority (21%) of the regions displaying de novo H3K27me3 in Y641F ESCs had no detectable H3K27me2 in WT ESCs, overlapped with regions featuring increased H3K27me3, and were assigned by proximity (± 20 kb) to genes whose expression was repressed in ESC-24h (Figure 3D). GO analysis of this gene list identified terms related to developmental processes (Figure 3D; Table S4), similar again to those identified in ESC-24h (Figure 1C; Table S3). During developmental lineage specification of mouse and human ESCs, H3K27me3 increases at intergenic regions (Hawkins et al., 2010; Pauler et al., 2009; Zhu et al., 2013). Our analysis further indicates that compared

to WT ESCs, the H3K27me3 signal in both ESC-24h and Y641F ESCs spreads laterally from the TSS and invades intergenic regions (Figures 3E–3G). In agreement with the H3K27me3 PCA results (Figure 3A), genomic H3K27me3 distribution in ESC-24h was more similar to that of Y641F ESCs than WT ESCs, with reduced representation at promoters and increased occupancy of intergenic regions (Figures 3F and 3G). Altogether, these findings reveal that H3K27me2 and H3K27me3 maps of Y641F ESCs resemble those of ESCs undergoing differentiation. This observation

***Ezh2*-Edited ESCs Preferentially Activate the Neural Fate Program and Are Refractory to the 2i-Induced Naive Ground State**

The distinct PRC2-mediated H3K27 methylation patterns observed prompted us to investigate potential differences between WT and Y641F ESCs. Immunostaining with an antibody directed against the pluripotent markers Pou5f1 (Oct4) (Nichols et al., 1998; Avilion et al., 2003) and mouse ESC-specific stage-specific embryonic antigen 1 (SSEA-1) indicated similar reactivity in WT and Y641F ESCs (Figure 4A). We employed fluorescence-activated cell sorting (FACS) analysis to more accurately gauge SSEA-1 expression and found it to be comparable in WT and Y641F ESCs (Figure 4B, left). Lastly, a growth curve analysis showed an equivalent proliferation rate for WT and Y641F ESCs (Figure 4B, right). Within these parameters, WT and Y641F ESCs are phenotypically indistinguishable.

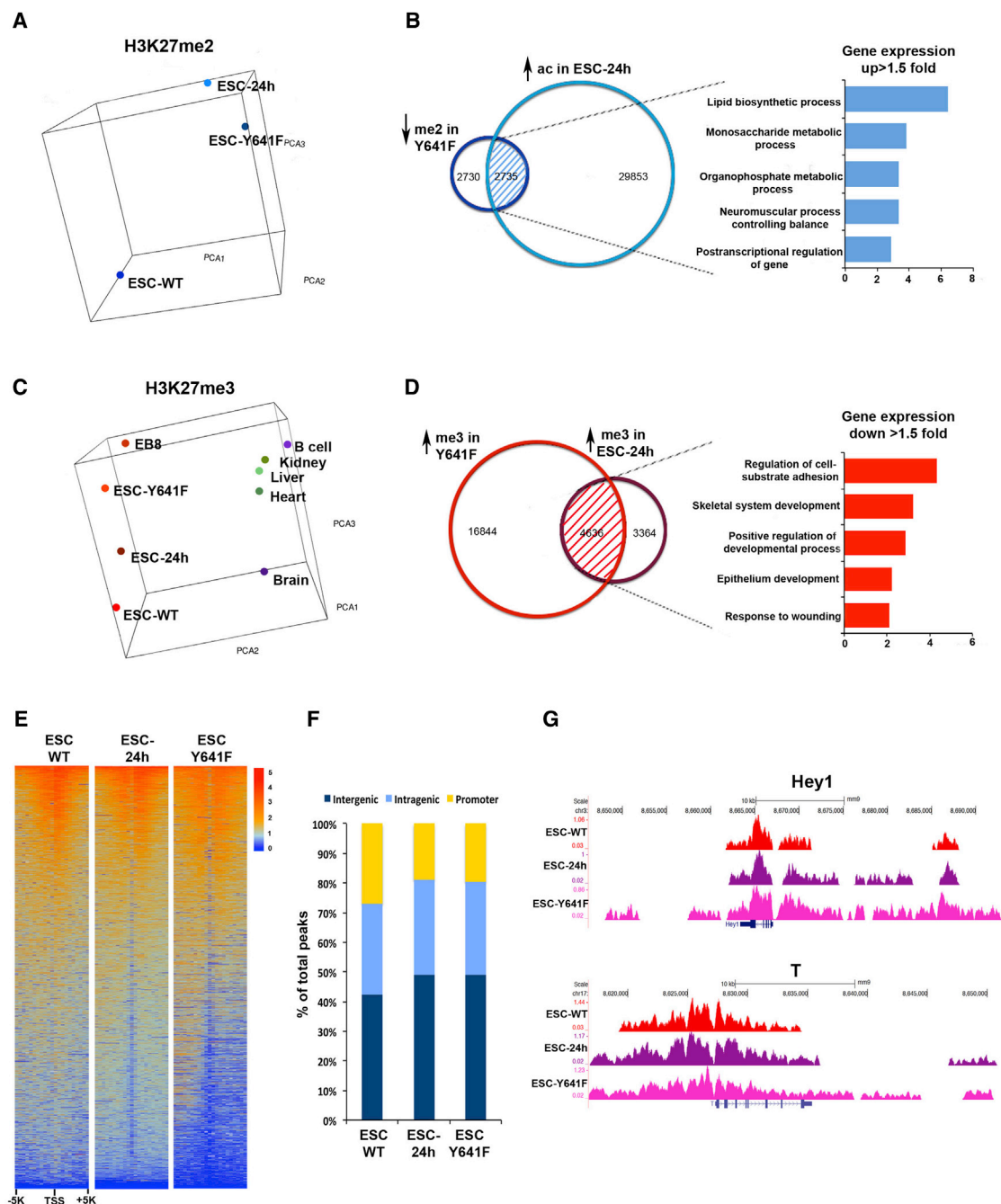


Figure 3. H3K27me2 and H3K27me3 States in *Ezh2*-Edited Y641F ESCs Resemble Those of Differentiating ESCs

(A) Three-dimensional principal component plots of H3K27me2 in ESC-WT, ESC-24h, and ESC-Y641F.

(B) GO-biological processes associated with genes within ± 20 kb of regions with decreased H3K27me2 in ESC-Y641F and increased H3K27ac in ESC-24h (shadowed area) and with ≥ 1.5 -fold increased expression in Y641F compared to WT ESCs.

(C) Three-dimensional principal-component plots of H3K27me3 in ESC-WT, ESC-24h, ESC-Y641F, day 8 embryoid bodies (EB8), and various cell or tissue types.

(D) GO-biological processes associated with genes within ± 20 kb of regions with increased H3K27me3 in ESC-Y641F and increased H3K27me3 in ESC-24h (shadowed area) and with ≥ 1.5 -fold decreased expression in Y641F compared to WT ESCs.

(E) Unsupervised clustering heatmap of H3K27me3 at genomic regions surrounding (± 5 kb) TSSs in ESC-WT, ESC-24h, and ESC-Y641F.

(F) Bar graphs depicting the distribution of H3K27me3 across genomic regions in ESC-WT, ESC-24h, and ESC-Y641F.

(G) H3K27me3 signal tracks for representative loci *Hey1* and *T* in ESC-WT, ESC-24h, and ESC-Y641F.

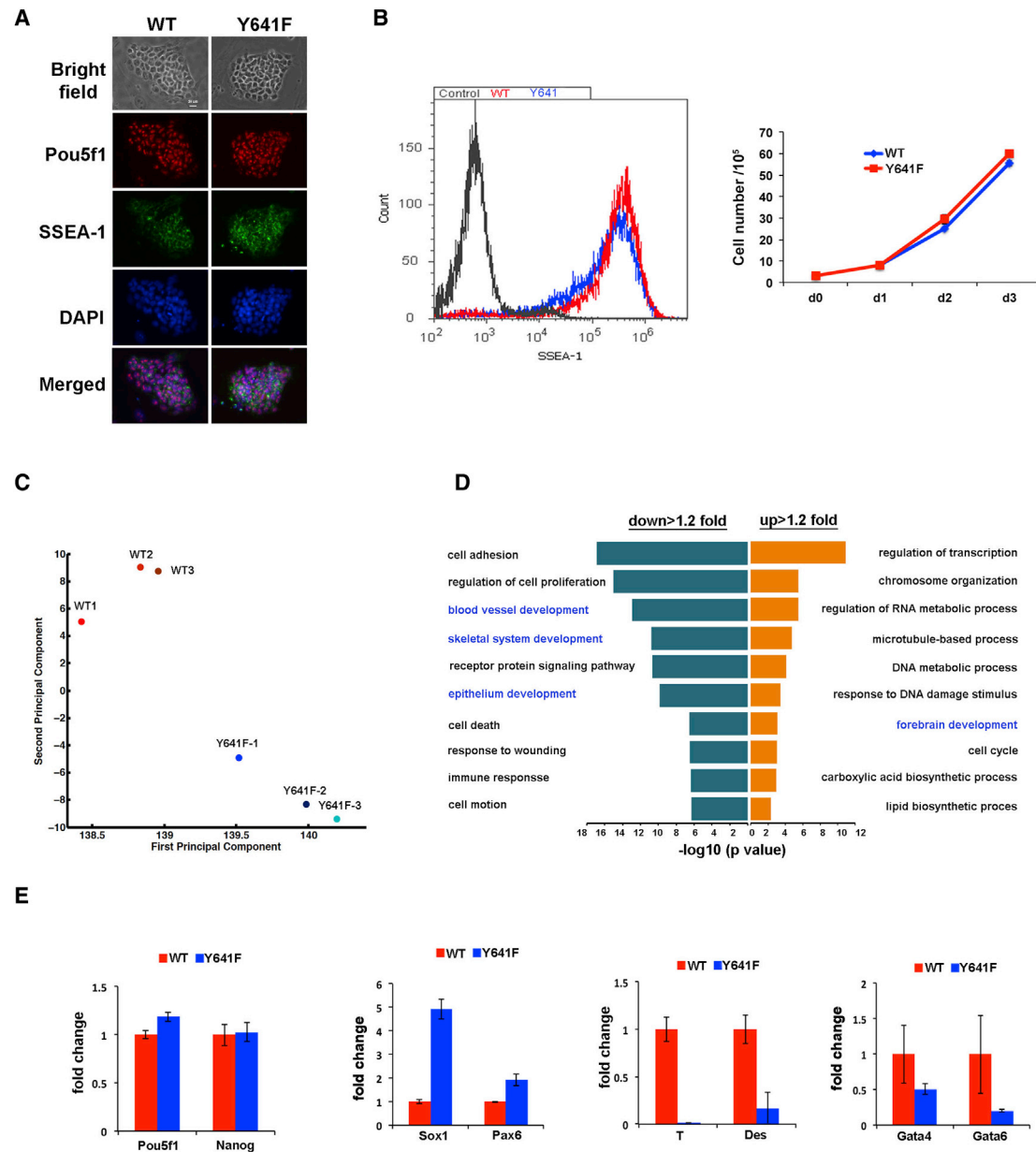


Figure 4. *Ezh2*-Edited ESCs Preferentially Activate the Neural Fate Program

(A) Morphology (bright field) and pluripotent marker (POU5F1 and SSEA-1) immunostaining of WT and Y641F ESCs.

(B) FACS analysis of SSEA-1 expression (left) and growth curve (right) of WT and Y641F ESCs.

(C) Two-dimensional principal-component plots of three RNA-seq biological replicates depicting gene expression profiles of WT and Y641F ESCs.

(D) GO-biological processes associated with genes with ≥ 1.2 -fold decreased (green bars) or increased (orange bars) expression in Y641F compared to WT ESCs.

(E) Fold-change expression (RPKM) from three RNA-seq biological replicates of pluripotent genes (*Pou5f1* and *Nanog*), neural genes (*Sox1* and *Pax6*), mesodermal genes (*T* and *Des*), and endodermal genes (*Gata4* and *Gata6*) between WT and Y641F ESCs. Data are presented as mean \pm SD.

Next, we performed RNA-seq on WT and Y641F ESCs cultured in conditions favoring maintenance of pluripotency. PCA of three independent RNA-seq biological replicates segregated WT and Y641F ESCs into two distinct expression profiles, indicating specific gene expression patterns in the two cell populations (Figure 4C). When considering developmental pro-

cesses, GO analysis of downregulated transcripts in Y641F ESCs returned terms related to mesoderm (blood vessel and skeletal) and epithelium development. Instead, forebrain development was a term represented in the categories of upregulated transcripts (Figure 4D; Table S4). We compared published mesodermal and neuronal gene signatures with those of control

and Y641F ESCs by gene set enrichment analysis (GSEA) (Subramanian et al., 2005). While the gene set from control ESCs (ES-WT) was anti-correlated, the Y641F ESCs gene set was positively correlated with cell-lineage-associated genes, especially with the signature for neural stem cells (Figure S5A). Motivated by these observations, we queried the expression of individual mesodermal and neural-specific transcripts. In concordance with immunostaining results, *Pou5f1* (*Oct4*) transcripts were similarly represented in WT and Y641F ESCs. Expression of *Nanog*, another core pluripotency factor (Mitsui et al., 2003; Chambers et al., 2003), was also comparable in WT and Y641F ESCs (Figure 4E; Table S1). In contrast, transcripts for *Sox1* and *Pax6*, two of the earliest neural markers (Mastick et al., 1997; Schwarz et al., 1999; Pevny et al., 1998; Wood and Episkopou, 1999), were increased, whereas mesodermal markers brachyury (*T*) and desmin (*Des*) and endodermal *Gata4* and *Gata6* transcripts were decreased in Y641F ESCs (Figure 4E; Table S1). Thus, while retaining expression of pluripotency factors, Y641F ESCs initiate expression of early neural genes and repress that of mesodermal and endodermal genes, even when cultured in a pluripotency-promoting medium.

Culturing ESCs in defined medium containing mitogen-activated protein/extracellular signal-related kinase (MEK) and glycogen synthase kinase 3 (GSK3) inhibitors (2i) reduces morphological heterogeneity and mosaic expression of pluripotency factors, mimics the environment of the mature mouse inner cell mass, and has allowed derivation of germline-competent ESCs from rats (Kalkan and Smith, 2014; Marks et al., 2012; Buehr et al., 2008). A lower expression of lineage-affiliated genes is consistent with acquisition of the naive ground state of 2i ESCs (Marks et al., 2012). To evaluate whether the transcriptome could be reprogrammed by 2i, we transferred serum-cultured control and Y641F ESCs to 2i medium and allowed them to adapt to the new culture conditions for two or three passages. Next, we generated and analyzed RNA-seq datasets from control and Y641F ESCs either cultured in serum or transferred to 2i. Pathway KEGG (Kyoto Encyclopedia of Genes and Genomes) analysis was employed to identify global transcriptional changes (Marks et al., 2012). From this analysis, it emerged that pathways enriched in 2i-control and Y641F ESCs were distinct (Figure 5A; Table S5). It was also evident that 2i-Y641F ESCs were enriched for pathways identified in ESCs cultured in either serum (pathways to cancer, focal adhesion) or 2i (glycolysis, propionate metabolism) (Table S5) (Marks et al., 2012). The most enriched pathway (axon guidance) was unique to 2i-Y641F ESCs (Figure 5A). Since expression of developmental regulators is affected by 2i (Marks et al., 2012), we queried this category of genes. Relative to serum conditions, naive factors *Nanog*, *Esrrb*, *Klf5*, and *Zfp42/Rex1*, along with pluripotent factors *Pou5f1* (*Oct4*) and *Sox2*, were modestly reduced in 2i Y641F ESCs (Figure 5B). Mesodermal and endodermal developmental regulators were overall decreased in Y641F ESCs cultured in either serum or 2i conditions. In contrast to control ESCs (Table S5) (Marks et al., 2012), expression of ectodermal regulators was generally increased in both serum and, with the exception of *Sox1*, 2i-Y641F ESCs (Figure 5B). When cultured in 2i medium, ESCs generate uniform, compact, and small dome-shaped refractile colonies. In contrast, ESCs in serum are heterogeneous in

morphology and flattened, with irregular borders and discernable individual cells (Wray et al., 2011; Marks et al., 2012). Accordingly, both control and Y641F ESCs cultured in serum or LIF and on feeders formed flattened colonies with discernable individual cells, whereas 2i conditions conferred morphological characteristics of the naive ground state only to WT ESCs. Y641F ESCs were partially refractory to 2i-induced morphological changes (Figure 5C). Altogether, enrichment of pathways upregulated in serum conditions, reduced expression of naive and pluripotent factors, increased expression of ectodermal regulators, and resistance to 2i-induced morphological changes suggest that Y641F ESCs, even when cultured in 2i conditions, retain transcriptional and morphological characteristics associated with a more primed or differentiated state.

The Neuronal Program Is Retained in *Ezh2*-Edited ESC-Derived Embryoid Bodies

We next asked whether the bias toward neural commitment displayed by Y641F ESCs was maintained at later stages of differentiation. Adherent WT and Y641F ESCs were cultured for 2 days in a medium (N2B27) supporting ESC differentiation to neural precursors (Ying et al., 2003). While *Pou5F1* levels decreased, expression of the neural markers *Sox1* and *Pax6* remained more elevated in Y641F ESCs (Figure S5B). To further investigate the developmental fate of Y641F ESCs, we plated WT and Y641F ESCs in conditions preventing adherence and isolated floating EBs after culturing them in suspension for 8 and 13 days, respectively. GO analysis of RNA-seq datasets identified genes transcripts involved in neuronal differentiation among those upregulated in both 8- and 13-day Y641F ESC-derived EBs (Figure 5D; Table S5). Finally, EBs were plated and allowed to adhere on a tissue culture dish for 4 days in standard culture conditions. EBs derived from WT ESCs displayed clear signs of mesoderm differentiation, as indicated by the presence of several fields of beating cardiomyocytes (Movie S1). Beating cardiomyocytes were instead not detectable in cultures of Y641F ESC-derived EBs (Figure 5E). In contrast, structures resembling neuronal projections and immunostaining positive for *Tuj1*, an antibody against neuron-specific class III β -tubulin, were prevalent in Y641F ESC-derived EBs (Figure 5E). Finally, we injected WT and Y641F ESCs into severe combined immunodeficiency (SCID) mice to induce teratoma formation. Histological analysis of teratomas revealed the presence of ectoderm, mesoderm, and endoderm derivatives (Figure S5C), indicating that Y641F ESCs retained developmental competency. Expression of neural transcripts *Sox1*, *Hes5*, and *Ngn1* was increased, while mesodermal brachyury (*T*) and endodermal *Gata4*, *Gata6*, and *Sox17* transcripts were decreased in teratomas derived from Y641F ESCs (Figure S5D). Overall, these findings document a propensity for ESCs with an increased H3K27me3/H3K27me2 ratio to acquire the neural cell fate.

Increased H3K27me3 and Transcriptional Repression of the TGF- β Pathway Underlies Neural Commitment of *Ezh2*-Edited ESCs

Vertebrate neuronal differentiation from uncommitted ESCs is initiated via cell-intrinsic mechanisms involving signals inhibiting the activity of pro-neuronal pathways (Hemmati-Brivanlou and

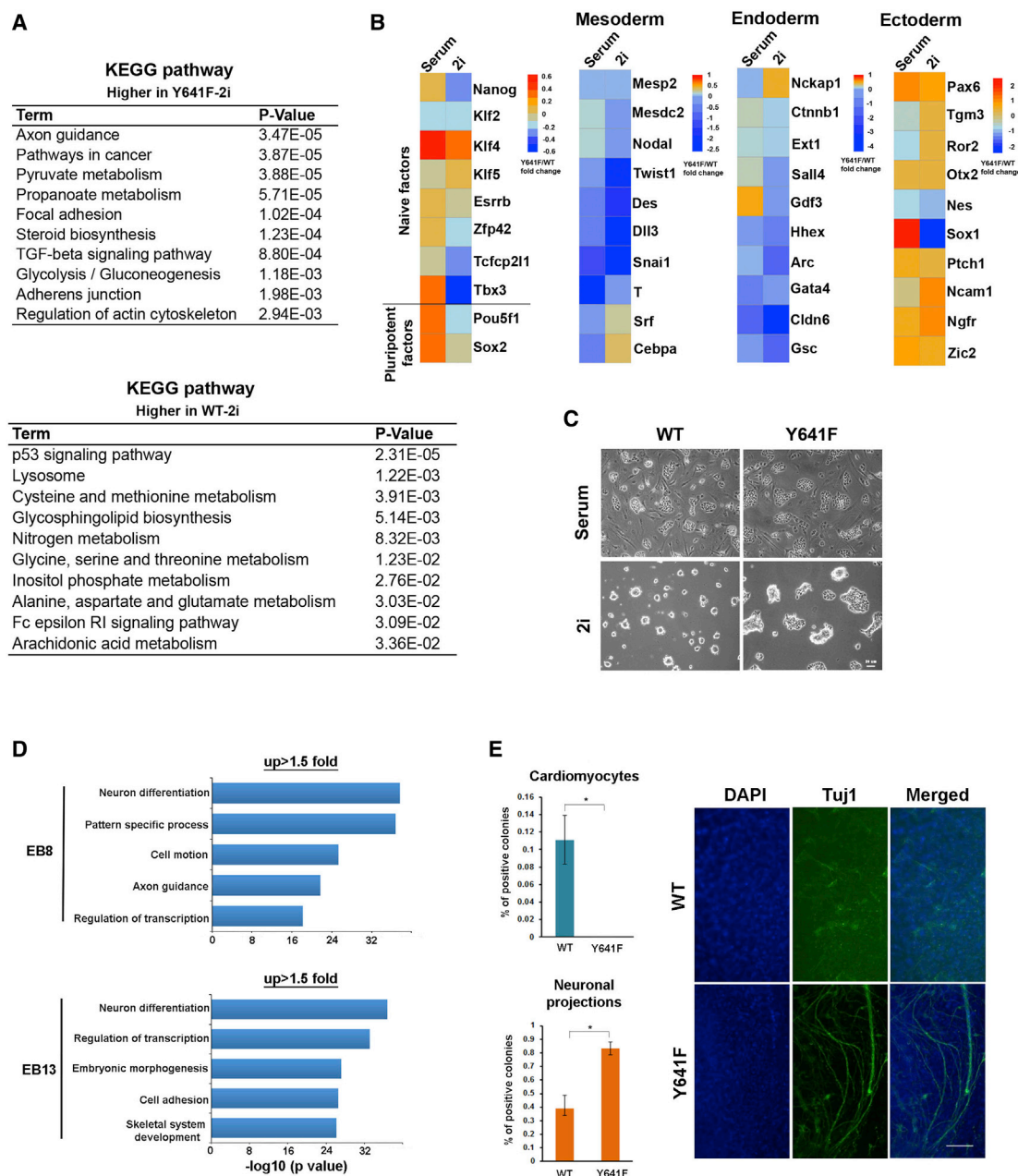


Figure 5. *Ezh2*-Edited ESCs Are Refractory to the 2i-Induced Naive Ground State and Retained Their Neural Program in Differentiating Embryoid Bodies

(A) Pathway KEGG analysis for genes with ≥ 1.2 -fold increased (top) or decreased (bottom) expression in Y641F compared to WT ESCs cultured in 2i medium. (B) Heatmap illustrating the RNA expression fold change between Y641F and WT cultured in serum and 2i medium for selected genes of different lineages. (C) Morphology of WT and Y641F ESCs cultured in 2i medium. (D) GO-biological processes associated with genes with ≥ 1.5 -fold increased expression in Y641F ESCs, EB8, or EB13 compared to WT EB8 or EB13. (E) Percentage of ESC colonies positive for beating cardiomyocytes (top left) or neuronal projections (bottom left), along with neural marker Tuj1 immunostaining of adherent EBs grown from WT or Y641F ESCs.

Melton, 1997). We reasoned that studying the pathways repressed in Y641F ESCs might provide novel insight into these mechanisms. Pathway KEGG analysis of RNA-seq datasets revealed that the transforming growth factor β (TGF- β) pathway was repressed in both ESC-24h and Y641F ESCs (Figures S6A

and 6A; Table S5). Inhibition of the TGF- β family of growth factors induces neuralization and brain formation in amphibians (Hemmati-Brivanlou and Melton, 1994; Reversade et al., 2005) and enhances ESC neuronal differentiation (Tropepe et al., 2001). Thus, we queried expression of TGF- β family members TGF β 1,

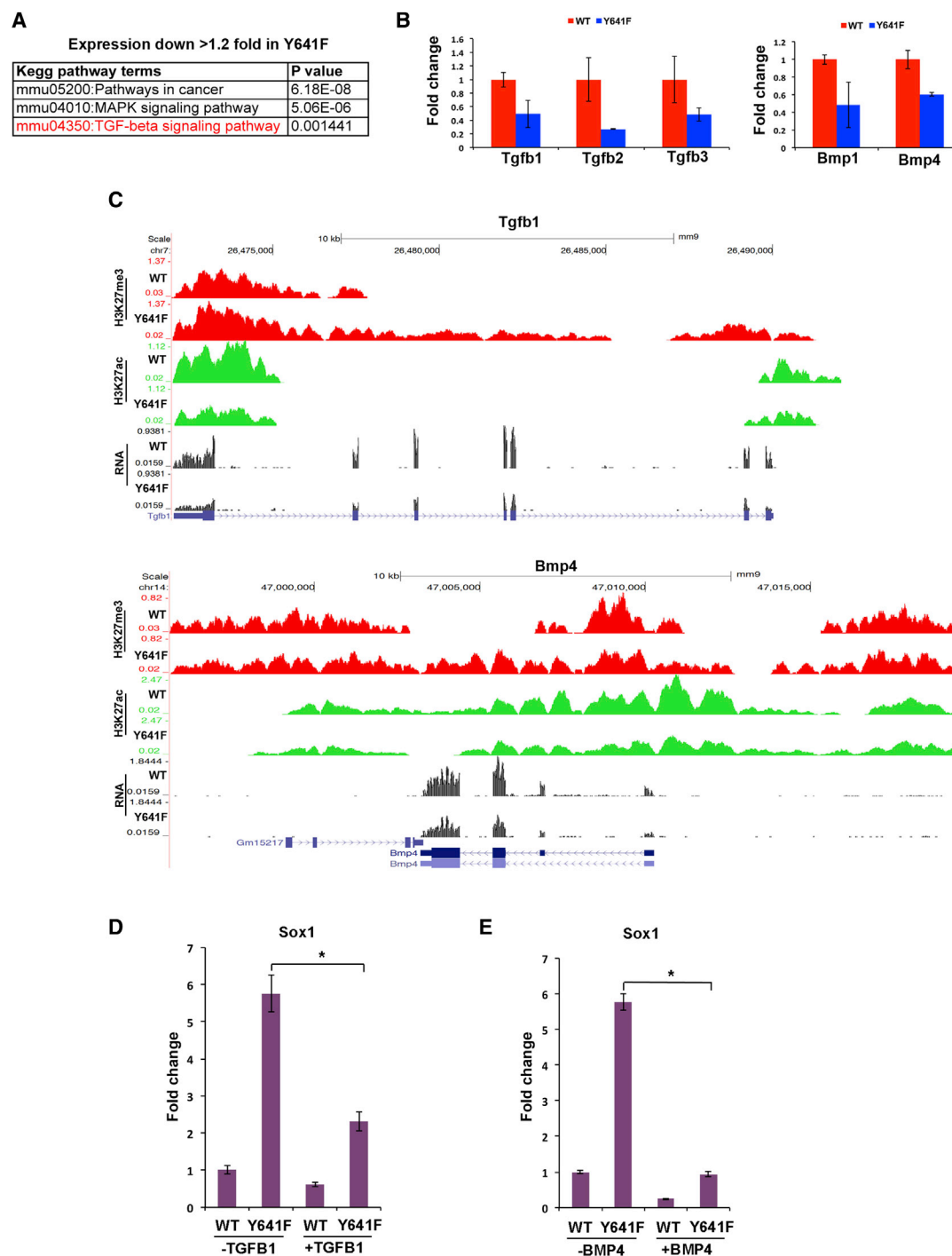


Figure 6. Increased H3K27me3 and Transcriptional Repression of the TGF- β Pathway Underlie Neural Commitment of *Ezh2*-Edited ESCs Cultured in Serum

(A) Pathway KEGG analysis for genes with ≥ 1.2 -fold increased expression in Y641F compared to WT ESCs.

(B) Fold-change expression (RPKM) from three RNA-seq biological replicates for TGF- β family members between WT and Y641F ESCs. Data are presented as mean \pm SD.

(C) H3K27me3 and H3K27ac signal tracks and RNA-seq traces at *TGF- β 1* and *BMP4* loci in WT and Y641F ESCs.

(D and E) Fold-change *Sox1* expression before or after the addition of TGF- β 1 (D) or BMP4 (E) recombinant proteins in WT and Y641F ESCs. Data are presented as mean \pm SD (n = 3).

TGF β 2, and TGF β 3, along with bone morphogenetic protein 1 (BMP1) and BMP4, and found their transcripts to be reduced in Y641F ESCs (Figure 6B). ChIP-seq and RNA-seq profiles of the *TGF β 1* and *BMP4* loci documented increased and de novo acquired H3K27me3, decreased H3K27ac, and reduced expression in Y641F ESCs (Figure 6C). Reduced *TGF β 1* and *BMP4* expression was also observed in ESC-24h (Figure S6B), suggesting a physiologic role for this phenomenon.

To establish whether repression of the TGF- β pathway was causally linked to increased expression of the neural marker *Sox1* (Figure 4E), we cultured WT and Y641F ESCs in the presence of either TGF β 1 or BMP4 recombinant protein. When exposed to either TGF- β factors, *Sox1* expression was specifically and significantly decreased in Y641F ESCs (Figures 6D and 6E). Thus, increased H3K27me3 at both the *TGF β 1* and *BMP4* loci is associated with their repression and *Sox1* activation in Y641F ESCs, while re-establishment of TGF β 1 and BMP4 signaling results in *Sox1* levels comparable to those observed in WT ESCs.

DISCUSSION

In ESCs, H3K27me3 is mainly enriched at bivalent promoters carrying H3K4me3 (Azuara et al., 2006; Bernstein et al., 2006). During the chromatin reorganization process accompanying ESC differentiation into somatic cells and tissues, H3K27me3 is re-distributed to much larger genomic areas (Pauler et al., 2009; Hawkins et al., 2010; Zhu et al., 2013). H3K27me3 reconfiguration may be related to the need for silencing inappropriate gene expression required for cell lineage specification. In addition to H3K27me3, PRC2 also catalyzes formation of the precursor H3K27me2 with a higher efficiency, a phenomenon reflected by the higher abundance of H3K27me2 compared to H3K27me3 in ESCs (Jung et al., 2010; Voigt et al., 2012).

In this study, we found the genome-wide distribution of H3K27me3 and H3K27me2 to differ in pluripotent and differentiating ESCs, with the two degrees of H3K27 methylation being enriched at functionally distinct genomic regulatory regions of different classes of genes. In pluripotent ESCs, H3K27me3⁺ regulatory regions are associated with developmental genes (Lee et al., 2006; Boyer et al., 2006), which tend to remain H3K27me3⁺ and repressed during initial ESC differentiation. On the other hand, we found H3K27me2 to be preferentially enriched at metabolic genes in pluripotent ESCs and replaced by acetylation in differentiating ESCs. Metabolic reprogramming of pluripotent stem cells is emerging as key regulator of energetics and epigenetics (Zhang et al., 2012; Ryall et al., 2015), and our findings indicate that H3K27me2 may play an important role in setting the transcriptional switch leading to metabolic reprogramming.

Without modifying the stoichiometry of the PRC2 subunits, we introduced, via TALEN-mediated genome editing, a single point mutation in one of the two *Ezh2* alleles of ESCs, causing *Ezh2* to preferentially trimethylate H3K27 and thus effectively altering the H3K27me3/H3K27me2 ratio. Genome-wide comparison of H3K27me3 and H3K27me2 maps in pluripotent and differentiating ESCs, along with *Ezh2*-edited (Y641F) ESCs, revealed several common features between differentiating ESCs and

Y641F ESCs. Previous reports have shown that H3K27me3 domains expand during ESC differentiation (Zhu et al., 2013; Wu et al., 2015). We found that, similar to ESC differentiation, H3K27me3 domains are also expanded in Y641F ESCs cultured in conditions favoring maintenance of pluripotency. While the majority of H3K27me3 domains were retained during ESC differentiation, H3K27me2 domains were preferentially resolved to either H3K27 acetylation or H3K27me3, suggesting a more plastic role of this histone mark as compared to H3K27me3. Importantly, preferential enrichment of H3K27me2 in pluripotent ESCs at metabolic genes destined to be H3K27 acetylated and activated in differentiating ESCs was recapitulated in Y641F ESCs, further suggesting the possibility that H3K27me2 might have a distinct and specific role in ESC metabolic reprogramming.

That the H3K27 PTMs experimentally generated by *Ezh2* Y641F mutation do occur during unperturbed ESC differentiation makes this model system of value for further investigation. While our findings clearly document a decreased H3K27me2/H3K27me3 ratio in both differentiating and Y641F ESCs, compared to pluripotent ESCs, a normalization strategy, such as that provided by ChIP with reference exogenous genome (ChIP-RX; Orlando et al., 2014), would be required to better assess quantitative H3K27 methylation dynamics.

The H3K27 methylation commonalities observed in differentiating ESCs and undifferentiated Y641F ESCs translated into transcriptome similarities between the two ESC. Even when maintained in culture conditions favoring pluripotency, Y641F ESCs initiated transcription of genes, such as *Sox1* and *Pax6*, indicative of early neural commitment. Because of the inherent tendency of ESCs cultured in serum to upregulate developmental regulators, we cultured the cells in 2i conditions which repress lineage-affiliated gene expression, rendering ESCs transcriptionally similar to pre-implantation naive epiblast cells (Boroviak et al., 2014; Ficiz et al., 2013; Habibi et al., 2013). 2i Y641F ESCs retained increased expression of ectodermal regulators and were refractory to 2i-induced morphological changes, which are characteristics suggestive of a primed or differentiating state. The TGF- β pathway was enriched in both control serum ESCs and 2i Y641F ESCs but downregulated in serum Y641F ESCs (Figures 5 and 6) (Marks et al., 2012). A possible interpretation of these findings is that upregulation of pathways that drive differentiation (e.g., TGF- β) is indicative of initial acquisition of differentiation potential in control serum and 2i Y641F ESCs. Further specification toward a more specialized neurogenic cell fate in serum Y641F ESCs would result in repression of the TGF- β pathway. In this sense, the bias toward neural commitment of serum Y641F ESCs was retained during differentiation, resulting in the formation of Y641F ESC-derived EBs with an overt neuronal phenotype and reduced representation of mesodermal derivatives. The observation that dissociated *Xenopus laevis* ectodermal cells acquire neural identity in the absence of instructive signals led to the proposal of a “neural default” model, which posits that the inhibition of an inhibitor drives neuralization of the ectoderm (Muñoz-Sanjuán and Brivanlou, 2002). As in amphibians, the default state of mouse ESCs is neural, and inhibition of TGF- β signaling promotes the transition from ESCs to primitive neural stem cells (Trophepe et al., 2001). Moreover, human ESCs can be differentiated into neuroectoderm-like

progenitors positive for Pax6 by inhibiting TGF- β and BMP (Gifford et al., 2013). In differentiating ESCs and Y641F ESCs, H3K27me3 at several members of the TGF- β superfamily was increased and their expression reduced compared to undifferentiated ESCs. Reactivation of the TGF- β pathway by exposing Y641F ESCs to either TGF β 1 or BMP4 returned Sox1 levels to those observed in control ESCs. Thus, modification of the H3K27me3/H3K27me2 ratio in Y641F ESCs results in gene expression mimicking that occurring during physiologic ESC differentiation.

Collectively, the observations reported here document genome-wide H3K27me2 and H3K27me3 maps of pluripotent and differentiating ESCs and ascribe a differential role to H3K27me3 and H3K27me2 in regulating the cell fate specification of ESCs. Since H3K27me1 was not affected in Y641F ESCs, it seems reasonable to propose that the differences observed in control and Y641F ESCs can be ascribed rather to a modified H3K27me2/H3K27me3 ratio. Ezh2 is present in distinct PRC2 complexes (Kuzmichev et al., 2004), and the presence or absence of defined PRC2-associated subunits influences its methylation efficiency (Sarma et al., 2008; Peng et al., 2009; Shen et al., 2009; Pasini et al., 2010; Li et al., 2010; Landeira et al., 2010; Sanulli et al., 2015). Thus, PRC2 composition may influence the degree of H3K27 methylation and, in doing so, participates in regulating ESC biology. If this is the case, in addition to sequential modulation of signaling pathways to direct the differentiation of pluripotent stem cells (Ben-Zvi and Melton, 2015), reagents affecting discrete H3K27 methylation states may be envisaged as tools to coax ESC differentiation into defined cell lineages.

EXPERIMENTAL PROCEDURES

Tissue Culture

Embryonic day 14 (E14) ESCs were grown initially on CF-1 MEF feeder (GlobalStem) and then passaged feeder-free on gelatin-coated dishes in ES medium (DMEM [Gibco], 15% HyClone fetal bovine serum [FBS] [GE Healthcare], GlutaMAX [Gibco], MEM nonessential amino acids [Gibco], sodium pyruvate [Gibco], LIF [Millipore; ESGRO], 0.1 mM β -mercaptoethanol, and antibiotics). For 24-hr differentiation, feeder-free ESCs were plated in low density (1×10^6 /10-cm plate) for 24 hr in ES medium (described above) without LIF and serum. For EB culture, 1×10^6 feeder-free ESCs were passaged onto 10-cm ultra-low-attachment culture dishes (Sigma). Serum-cultured ESCs were converted to ground state by culturing and passaging the cells in ESGRO-2i medium (Millipore, #SF016-100) following the manufacturer's instructions. EBs were maintained in 15% HyClone FBS, MEM nonessential amino acids, and sodium pyruvate. For adherent culture, three EBs were collected and plated per well in gelatin-coated six-well plates. Adherent EBs were differentiated in 10% HyClone FBS, 5% horse serum (Gibco), GlutaMAX, MEM nonessential amino acids, and 0.1 mM β -mercaptoethanol. For culture in N2B27 neural differentiation media, 3×10^5 feeder-free ESCs were passaged onto gelatin-coated 10-cm culture dishes. The following day, dishes were changed to N2B27 media (1:1 ratio of Neurobasal:DMEM/Ham's F-12 [Life Technologies] supplemented with 1:200 N2 [Life Technologies], 1:100 B27 [Life Technologies], and 0.1 mM β -mercaptoethanol). C2C12 myoblasts were maintained in DMEM medium with 20% FBS (Gibco) as previously described (Mousavi et al., 2012).

Culture with Recombinant Proteins

ESCs were seeded feeder-free at a concentration of 1.8×10^6 per 10-cm gelatin-coated dish. The following day, normal ES media was supplemented with either recombinant mouse Tgfb1 (R&D Systems, 240-B-010) or Bmp4

(R&D, 5020-BP-010) protein at a concentration of 30 ng/mL or 40 ng/mL, respectively.

Analysis of Cell Growth

To generate cell growth curves, ESCs (3×10^5) were seeded in triplicate onto six-well gelatin-coated dishes on day 0. Cells were harvested and counted via Cellometer K2 Image Cytometer (Nexcelom Bioscience) every day for 3 days.

Teratoma Formation and Analysis

A description of teratoma formation and analysis is provided in [Supplemental Experimental Procedures](#).

RNA Expression Analysis

A description of RNA expression analysis by qPCR is provided in [Supplemental Experimental Procedures](#).

Western Blot Analysis

A description of western blot analysis is provided in [Supplemental Experimental Procedures](#).

Antibody Specificity Analysis

A description of antibody specificity analysis is provided in [Supplemental Experimental Procedures](#).

Immunofluorescence

A description of immunofluorescence of ESC and adherent EBs is reported in [Supplemental Experimental Procedures](#).

Flow Cytometry

A description of flow cytometry of ESC is provided in [Supplemental Experimental Procedures](#).

Mass Spectrometry

A description of mass spectrometry of histone H3 is provided in [Supplemental Experimental Procedures](#).

RNA-Seq

A description of RNA-seq procedures is provided in [Supplemental Experimental Procedures](#).

ChIP-Seq

A description of ChIP-seq procedures is provided in [Supplemental Experimental Procedures](#).

ChIP-Seq and RNA-Seq Data Analysis

Descriptions of data processing and bioinformatic analyses, including tag density, 6-mer analysis, motif enrichment, PCA, and heatmap analysis are provided in [Supplemental Experimental Procedures](#).

TALEN Generation and Genome Editing

A description of TALEN and Ezh2Y641F donor construction, along with genome editing in ESCs, is provided in [Supplemental Experimental Procedures](#).

Antibodies

A detailed list of antibodies is available in [Table S1](#).

ACCESSION NUMBERS

The accession number for the ChIP-seq and RNA-seq datasets reported in this paper is GEO: GSE85717.

SUPPLEMENTAL INFORMATION

Supplemental Information includes Supplemental Experimental Procedures, six figures, five tables, and one movie and can be found with this article online at <http://dx.doi.org/10.1016/j.celrep.2016.09.087>.

AUTHOR CONTRIBUTIONS

A.H.J., S.W., and V.S. conceived and designed the overall project and wrote the manuscript with input from the other authors. A.H.J. and S.W. performed most of the experiments. K.D.K. and H.Z. designed and conducted computational analysis. P.-F.T., X.F., K.O.V., A.A., G.G.-C. J.K., S.S., and A.L.K. performed tissue culture, immunostaining, and mass spectrometry experiments. J.Z. performed TALEN experiments. R.A.P., B.A.G., and R.C. provided advice and technical support. All authors have read and approved the manuscript.

ACKNOWLEDGMENTS

We thank Prof. J.B. Gurdon and members of his laboratory in Cambridge, UK for hosting S.W. during the initial part of this work. We also thank the personnel of the NIAMS Sequencing, Light Imaging, and Flow Cytometry Facilities and of the NHLBI Transgenic and Pathology Cores at the National Institutes of Health (NIH). S.W. was supported in part by fellowships from the Gates Cambridge Trust and NIH-Cambridge MD/PhD Program. S.S. and B.A.G. were supported by a grant from the NIH (GM110174). This research was supported in part by the Intramural Research Program of the NIAMS at the NIH.

Received: December 23, 2015

Revised: September 7, 2016

Accepted: September 26, 2016

Published: October 25, 2016

REFERENCES

- Avilion, A.A., Nicolis, S.K., Pevny, L.H., Perez, L., Vivian, N., and Lovell-Badge, R. (2003). Multipotent cell lineages in early mouse development depend on SOX2 function. *Genes Dev.* 17, 126–140.
- Azuara, V., Perry, P., Sauer, S., Spivakov, M., Jørgensen, H.F., John, R.M., Gouti, M., Casanova, M., Warnes, G., Merkschlager, M., and Fisher, A.G. (2006). Chromatin signatures of pluripotent cell lines. *Nat. Cell Biol.* 8, 532–538.
- Banaszynski, L.A., Wen, D., Dewell, S., Whitcomb, S.J., Lin, M., Diaz, N., Elsässer, S.J., Chappier, A., Goldberg, A.D., Canaani, E., et al. (2013). Hira-dependent histone H3.3 deposition facilitates PRC2 recruitment at developmental loci in ES cells. *Cell* 155, 107–120.
- Barsotti, A.M., Ryskin, M., Zhong, W., Zhang, W.G., Giannakou, A., Loreth, C., Diesl, V., Follettie, M., Golas, J., Lee, M., et al. (2015). Epigenetic reprogramming by tumor-derived EZH2 gain-of-function mutations promotes aggressive 3D cell morphologies and enhances melanoma tumor growth. *Oncotarget* 6, 2928–2938.
- Ben-Zvi, D., and Melton, D.A. (2015). Modeling human nutrition using human embryonic stem cells. *Cell* 161, 12–17.
- Bernstein, B.E., Mikkelsen, T.S., Xie, X., Kamal, M., Huebert, D.J., Cuff, J., Fry, B., Meissner, A., Wernig, M., Plath, K., et al. (2006). A bivalent chromatin structure marks key developmental genes in embryonic stem cells. *Cell* 125, 315–326.
- Bogdanove, A.J., and Voytas, D.F. (2011). TAL effectors: customizable proteins for DNA targeting. *Science* 333, 1843–1846.
- Boroviak, T., Loos, R., Bertone, P., Smith, A., and Nichols, J. (2014). The ability of inner-cell-mass cells to self-renew as embryonic stem cells is acquired following epiblast specification. *Nat. Cell Biol.* 16, 516–528.
- Boyer, L.A., Plath, K., Zeitlinger, J., Brambrink, T., Medeiros, L.A., Lee, T.I., Levine, S.S., Wernig, M., Tajonar, A., Ray, M.K., et al. (2006). Polycomb complexes repress developmental regulators in murine embryonic stem cells. *Nature* 441, 349–353.
- Buehr, M., Meek, S., Blair, K., Yang, J., Ure, J., Silva, J., McLay, R., Hall, J., Ying, Q.L., and Smith, A. (2008). Capture of authentic embryonic stem cells from rat blastocysts. *Cell* 135, 1287–1298.
- Chamberlain, S.J., Yee, D., and Magnuson, T. (2008). Polycomb repressive complex 2 is dispensable for maintenance of embryonic stem cell pluripotency. *Stem Cells* 26, 1496–1505.
- Chambers, I., Colby, D., Robertson, M., Nichols, J., Lee, S., Tweedie, S., and Smith, A. (2003). Functional expression cloning of Nanog, a pluripotency sustaining factor in embryonic stem cells. *Cell* 113, 643–655.
- Collins, R.E., Tachibana, M., Tamaru, H., Smith, K.M., Jia, D., Zhang, X., Selker, E.U., Shinkai, Y., and Cheng, X. (2005). In vitro and in vivo analyses of a Phe/Tyr switch controlling product specificity of histone lysine methyltransferases. *J. Biol. Chem.* 280, 5563–5570.
- Cui, K., Zang, C., Roh, T.Y., Schones, D.E., Childs, R.W., Peng, W., and Zhao, K. (2009). Chromatin signatures in multipotent human hematopoietic stem cells indicate the fate of bivalent genes during differentiation. *Cell Stem Cell* 4, 80–93.
- Ferrari, K.J., Scelfo, A., Jammula, S., Cuomo, A., Barozzi, I., Stützer, A., Fischle, W., Bonaldi, T., and Pasini, D. (2014). Polycomb-dependent H3K27me1 and H3K27me2 regulate active transcription and enhancer fidelity. *Mol. Cell* 53, 49–62.
- Ficz, G., Hore, T.A., Santos, F., Lee, H.J., Dean, W., Arand, J., Krueger, F., Oxley, D., Paul, Y.L., Walter, J., et al. (2013). FGF signaling inhibition in ESCs drives rapid genome-wide demethylation to the epigenetic ground state of pluripotency. *Cell Stem Cell* 13, 351–359.
- Gifford, C.A., Ziller, M.J., Gu, H., Trapnell, C., Donaghey, J., Tsankov, A., Shalek, A.K., Kelley, D.R., Shishkin, A.A., Issner, R., et al. (2013). Transcriptional and epigenetic dynamics during specification of human embryonic stem cells. *Cell* 153, 1149–1163.
- Habibi, E., Brinkman, A.B., Arand, J., Kroeze, L.I., Kerstens, H.H., Matarese, F., Lepikhov, K., Gut, M., Brun-Heath, I., Hubner, N.C., et al. (2013). Whole-genome bisulfite sequencing of two distinct interconvertible DNA methylomes of mouse embryonic stem cells. *Cell Stem Cell* 13, 360–369.
- Hawkins, R.D., Hon, G.C., Lee, L.K., Ngo, Q., Lister, R., Pelizzola, M., Edsall, L.E., Kuan, S., Luu, Y., Klugman, S., et al. (2010). Distinct epigenomic landscapes of pluripotent and lineage-committed human cells. *Cell Stem Cell* 6, 479–491.
- Heintzman, N.D., Stuart, R.K., Hon, G., Fu, Y., Ching, C.W., Hawkins, R.D., Barrera, L.O., Van Calcar, S., Qu, C., Ching, K.A., et al. (2007). Distinct and predictive chromatin signatures of transcriptional promoters and enhancers in the human genome. *Nat. Genet.* 39, 311–318.
- Hemmati-Brivanlou, A., and Melton, D.A. (1994). Inhibition of activin receptor signaling promotes neuralization in *Xenopus*. *Cell* 77, 273–281.
- Hemmati-Brivanlou, A., and Melton, D. (1997). Vertebrate neural induction. *Annu. Rev. Neurosci.* 20, 43–60.
- Jung, H.R., Pasini, D., Helin, K., and Jensen, O.N. (2010). Quantitative mass spectrometry of histones H3.2 and H3.3 in Suz12-deficient mouse embryonic stem cells reveals distinct, dynamic post-translational modifications at Lys-27 and Lys-36. *Mol. Cell. Proteomics* 9, 838–850.
- Kalkan, T., and Smith, A. (2014). Mapping the route from naive pluripotency to lineage specification. *Philos. Trans. R. Soc. Lond. B Biol. Sci.* 369, 20130540.
- Kuzmichev, A., Jenuwein, T., Tempst, P., and Reinberg, D. (2004). Different EZH2-containing complexes target methylation of histone H1 or nucleosomal histone H3. *Mol. Cell* 14, 183–193.
- Landeira, D., Sauer, S., Poot, R., Dvorkina, M., Mazzarella, L., Jørgensen, H.F., Pereira, C.F., Leleu, M., Piccolo, F.M., Spivakov, M., et al. (2010). Jarid2 is a PRC2 component in embryonic stem cells required for multi-lineage differentiation and recruitment of PRC1 and RNA Polymerase II to developmental regulators. *Nat. Cell Biol.* 12, 618–624.
- Lee, T.I., Jenner, R.G., Boyer, L.A., Guenther, M.G., Levine, S.S., Kumar, R.M., Chevalier, B., Johnstone, S.E., Cole, M.F., Isono, K., et al. (2006). Control of developmental regulators by Polycomb in human embryonic stem cells. *Cell* 125, 301–313.
- Lee, H.G., Kahn, T.G., Simcox, A., Schwartz, Y.B., and Pirrotta, V. (2015). Genome-wide activities of Polycomb complexes control pervasive transcription. *Genome Res.* 25, 1170–1181.
- Leeb, M., Pasini, D., Novatchkova, M., Jaritz, M., Helin, K., and Wutz, A. (2010). Polycomb complexes act redundantly to repress genomic repeats and genes. *Genes Dev.* 24, 265–276.

- Li, G., Margueron, R., Ku, M., Chambon, P., Bernstein, B.E., and Reinberg, D. (2010). Jarid2 and PRC2, partners in regulating gene expression. *Genes Dev.* 24, 368–380.
- Margueron, R., and Reinberg, D. (2011). The Polycomb complex PRC2 and its mark in life. *Nature* 469, 343–349.
- Marks, H., Kalkan, T., Menafrá, R., Denissov, S., Jones, K., Hofmeister, H., Nichols, J., Kranz, A., Stewart, A.F., Smith, A., and Stunnenberg, H.G. (2012). The transcriptional and epigenomic foundations of ground state pluripotency. *Cell* 149, 590–604.
- Mastick, G.S., Davis, N.M., Andrew, G.L., and Easter, S.S., Jr. (1997). Pax-6 functions in boundary formation and axon guidance in the embryonic mouse forebrain. *Development* 124, 1985–1997.
- McCabe, M.T., Graves, A.P., Ganji, G., Diaz, E., Halsey, W.S., Jiang, Y., Smitheman, K.N., Ott, H.M., Pappalardi, M.B., Allen, K.E., et al. (2012). Mutation of A677 in histone methyltransferase EZH2 in human B-cell lymphoma promotes hypertrimethylation of histone H3 on lysine 27 (H3K27). *Proc. Natl. Acad. Sci. USA* 109, 2989–2994.
- Mitsui, K., Tokuzawa, Y., Itoh, H., Segawa, K., Murakami, M., Takahashi, K., Maruyama, M., Maeda, M., and Yamanaka, S. (2003). The homeoprotein Nanog is required for maintenance of pluripotency in mouse epiblast and ES cells. *Cell* 113, 631–642.
- Montgomery, N.D., Yee, D., Chen, A., Kalantry, S., Chamberlain, S.J., Otte, A.P., and Magnuson, T. (2005). The murine polycomb group protein Eed is required for global histone H3 lysine-27 methylation. *Curr. Biol.* 15, 942–947.
- Mousavi, K., Zare, H., Wang, A.H., and Sartorelli, V. (2012). Polycomb protein Ezh1 promotes RNA polymerase II elongation. *Mol. Cell* 45, 255–262.
- Muñoz-Sanjuán, I., and Brivanlou, A.H. (2002). Neural induction, the default model and embryonic stem cells. *Nat. Rev. Neurosci.* 3, 271–280.
- Nichols, J., Zevnik, B., Anastasiadis, K., Niwa, H., Klewe-Nebenius, D., Chambers, I., Schöler, H., and Smith, A. (1998). Formation of pluripotent stem cells in the mammalian embryo depends on the POU transcription factor Oct4. *Cell* 95, 379–391.
- Onder, T.T., Kara, N., Cherry, A., Sinha, A.U., Zhu, N., Bernt, K.M., Cahan, P., Marcarci, B.O., Unternaehrer, J., Gupta, P.B., et al. (2012). Chromatin-modifying enzymes as modulators of reprogramming. *Nature* 483, 598–602.
- Orlando, D.A., Chen, M.W., Brown, V.E., Solanki, S., Choi, Y.J., Olson, E.R., Fritz, C.C., Bradner, J.E., and Guenther, M.G. (2014). Quantitative ChIP-Seq normalization reveals global modulation of the epigenome. *Cell Rep.* 9, 1163–1170.
- Pasini, D., Bracken, A.P., Hansen, J.B., Capillo, M., and Helin, K. (2007). The polycomb group protein Suz12 is required for embryonic stem cell differentiation. *Mol. Cell. Biol.* 27, 3769–3779.
- Pasini, D., Cloos, P.A., Walfridsson, J., Olsson, L., Bukowski, J.P., Johansen, J.V., Bak, M., Tommerup, N., Rappsilber, J., and Helin, K. (2010). JARID2 regulates binding of the Polycomb repressive complex 2 to target genes in ES cells. *Nature* 464, 306–310.
- Pauler, F.M., Sloane, M.A., Huang, R., Regha, K., Koerner, M.V., Tamir, I., Sommer, A., Aszodi, A., Jenuwein, T., and Barlow, D.P. (2009). H3K27me3 forms BLOCs over silent genes and intergenic regions and specifies a histone banding pattern on a mouse autosomal chromosome. *Genome Res.* 19, 221–233.
- Peng, J.C., Valouev, A., Swigut, T., Zhang, J., Zhao, Y., Sidow, A., and Wysocka, J. (2009). Jarid2/Jumonji coordinates control of PRC2 enzymatic activity and target gene occupancy in pluripotent cells. *Cell* 139, 1290–1302.
- Pevny, L.H., Sockanathan, S., Placzek, M., and Lovell-Badge, R. (1998). A role for SOX1 in neural determination. *Development* 125, 1967–1978.
- Reversade, B., Kuroda, H., Lee, H., Mays, A., and De Robertis, E.M. (2005). Depletion of Bmp2, Bmp4, Bmp7 and Spemann organizer signals induces massive brain formation in *Xenopus* embryos. *Development* 132, 3381–3392.
- Rising, E.M., Comet, I., Leblanc, B., Wu, X., Johansen, J.V., and Helin, K. (2014). Gene silencing triggers polycomb repressive complex 2 recruitment to CpG islands genome wide. *Mol. Cell* 55, 347–360.
- Ryall, J.G., Cliff, T., Dalton, S., and Sartorelli, V. (2015). Metabolic reprogramming of stem cell epigenetics. *Cell Stem Cell* 17, 651–662.
- Sanulli, S., Justin, N., Teissandier, A., Ancelin, K., Portoso, M., Caron, M., Michaud, A., Lombard, B., da Rocha, S.T., Offer, J., et al. (2015). Jarid2 methylation via the PRC2 complex regulates H3K27me3 deposition during cell differentiation. *Mol. Cell* 57, 769–783.
- Sarma, K., Margueron, R., Ivanov, A., Pirrotta, V., and Reinberg, D. (2008). Ezh2 requires PHF1 to efficiently catalyze H3 lysine 27 trimethylation in vivo. *Mol. Cell. Biol.* 28, 2718–2731.
- Schwarz, M., Alvarez-Bolado, G., Dressler, G., Urbánec, P., Busslinger, M., and Gruss, P. (1999). Pax2/5 and Pax6 subdivide the early neural tube into three domains. *Mech. Dev.* 82, 29–39.
- Shen, X., Liu, Y., Hsu, Y.J., Fujiwara, Y., Kim, J., Mao, X., Yuan, G.C., and Orkin, S.H. (2008). EZH1 mediates methylation on histone H3 lysine 27 and complements EZH2 in maintaining stem cell identity and executing pluripotency. *Mol. Cell* 32, 491–502.
- Shen, X., Kim, W., Fujiwara, Y., Simon, M.D., Liu, Y., Mysliwiec, M.R., Yuan, G.C., Lee, Y., and Orkin, S.H. (2009). Jumoni modulates polycomb activity and self-renewal versus differentiation of stem cells. *Cell* 139, 1303–1314.
- Souroullas, G.P., Jeck, W.R., Parker, J.S., Simon, J.M., Liu, J.Y., Paulk, J., Xiong, J., Clark, K.S., Fedorow, Y., Qi, J., et al. (2016). An oncogenic Ezh2 mutation induces tumors through global redistribution of histone 3 lysine 27 trimethylation. *Nat. Med.* 22, 632–640.
- Steiner, L.A., Schulz, V.P., Maksimova, Y., Wong, C., and Gallagher, P.G. (2011). Patterns of histone H3 lysine 27 monomethylation and erythroid cell type-specific gene expression. *J. Biol. Chem.* 286, 39457–39465.
- Subramanian, A., Tamayo, P., Mootha, V.K., Mukherjee, S., Ebert, B.L., Gillette, M.A., Paulovich, A., Pomeroy, S.L., Golub, T.R., Lander, E.S., and Mesirov, J.P. (2005). Gene set enrichment analysis: a knowledge-based approach for interpreting genome-wide expression profiles. *Proc. Natl. Acad. Sci. USA* 102, 15545–15550.
- Tropepe, V., Hitoshi, S., Sirard, C., Mak, T.W., Rossant, J., and van der Kooy, D. (2001). Direct neural fate specification from embryonic stem cells: a primitive mammalian neural stem cell stage acquired through a default mechanism. *Neuron* 30, 65–78.
- Voigt, P., LeRoy, G., Drury, W.J., 3rd, Zee, B.M., Son, J., Beck, D.B., Young, N.L., Garcia, B.A., and Reinberg, D. (2012). Asymmetrically modified nucleosomes. *Cell* 151, 181–193.
- Wood, H.B., and Episkopou, V. (1999). Comparative expression of the mouse Sox1, Sox2 and Sox3 genes from pre-gastrulation to early somite stages. *Mech. Dev.* 86, 197–201.
- Wray, J., Kalkan, T., Gomez-Lopez, S., Eckardt, D., Cook, A., Kemler, R., and Smith, A. (2011). Inhibition of glycogen synthase kinase-3 alleviates Tcf3 repression of the pluripotency network and increases embryonic stem cell resistance to differentiation. *Nat. Cell Biol.* 13, 838–845.
- Wu, J., Okamura, D., Li, M., Suzuki, K., Luo, C., Ma, L., He, Y., Li, Z., Benner, C., Tamura, I., et al. (2015). An alternative pluripotent state confers interspecies chimaeric competency. *Nature* 521, 316–321.
- Yap, D.B., Chu, J., Berg, T., Schapira, M., Cheng, S.W., Moradian, A., Morin, R.D., Mungall, A.J., Meissner, B., Boyle, M., et al. (2011). Somatic mutations at EZH2 Y641 act dominantly through a mechanism of selectively altered PRC2 catalytic activity, to increase H3K27 trimethylation. *Blood* 117, 2451–2459.
- Ying, Q.L., Stavridis, M., Griffiths, D., Li, M., and Smith, A. (2003). Conversion of embryonic stem cells into neuroectodermal precursors in adherent monoculture. *Nat. Biotechnol.* 21, 183–186.
- Zhang, J., Nuebel, E., Daley, G.Q., Koehler, C.M., and Teitell, M.A. (2012). Metabolic regulation in pluripotent stem cells during reprogramming and self-renewal. *Cell Stem Cell* 11, 589–595.
- Zhu, J., Adli, M., Zou, J.Y., Verstappen, G., Coyne, M., Zhang, X., Durham, T., Miri, M., Deshpande, V., De Jager, P.L., et al. (2013). Genome-wide chromatin state transitions associated with developmental and environmental cues. *Cell* 152, 642–654.